Figure 5.

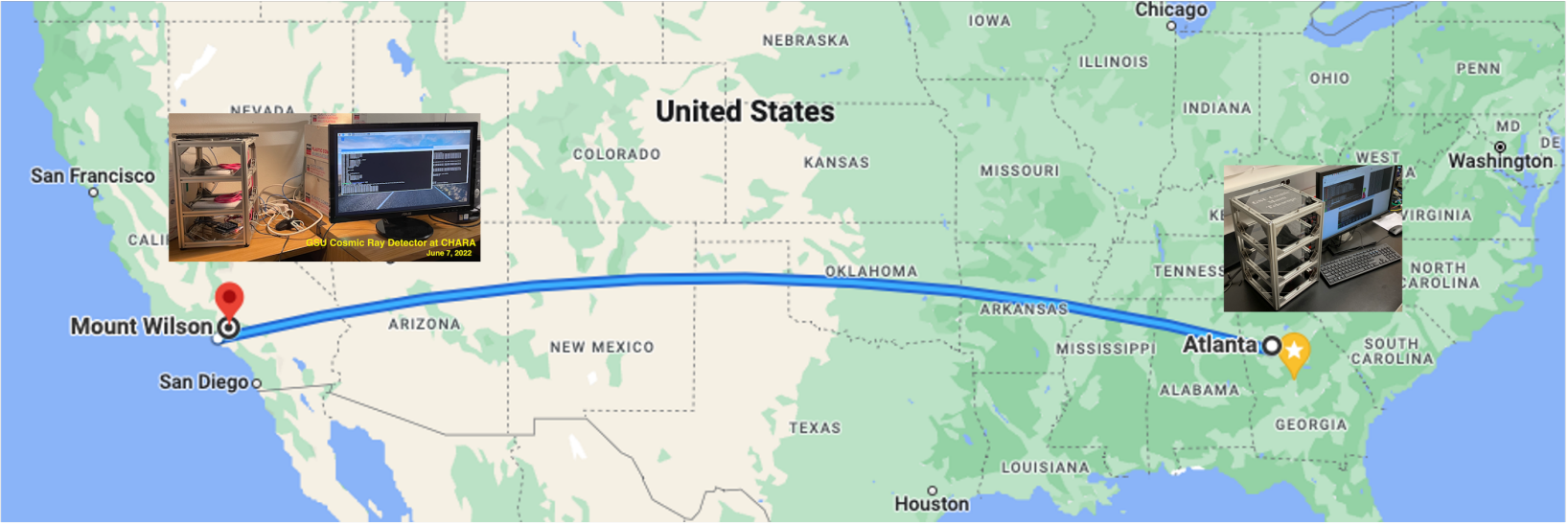

33° 30' 13.095" S 150° 22' 37.368" E

Mt Wilson Observatory Altitude: 1,742 m

33° 44' 56.383" N 84° 23' 16.737" W

Atlanta Altitude: 336 m

Figure 7.

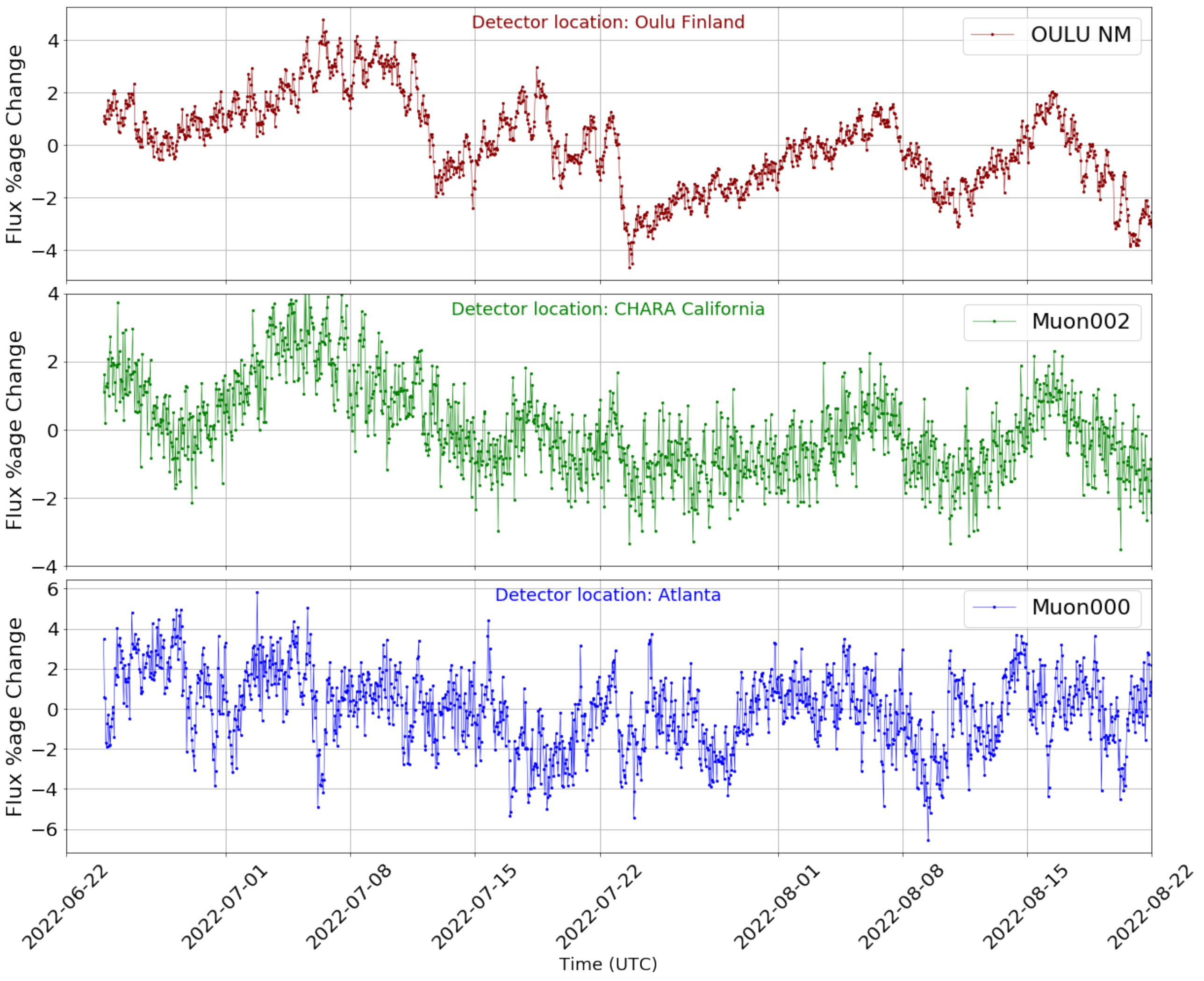
Detector location: Oulu Finland
OULU NM
Detector location: CHARA California
Muon002
Detector location: Atlanta
Muon000
Flux %age Change
Time (UTC)
2022-06-22
2022-07-01
2022-07-08
2022-07-15
2022-07-22
2022-08-01
2022-08-08
2022-08-15
2022-08-22

Figure 1.

(1) Primary cosmic ray particle has galactic origin

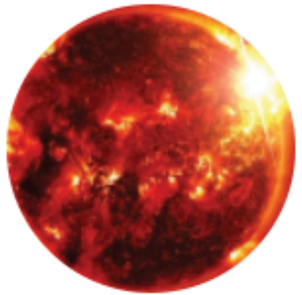

(2) Amount of cosmic ray particles reaching the top of the earth atmosphere is affected by solar activities.

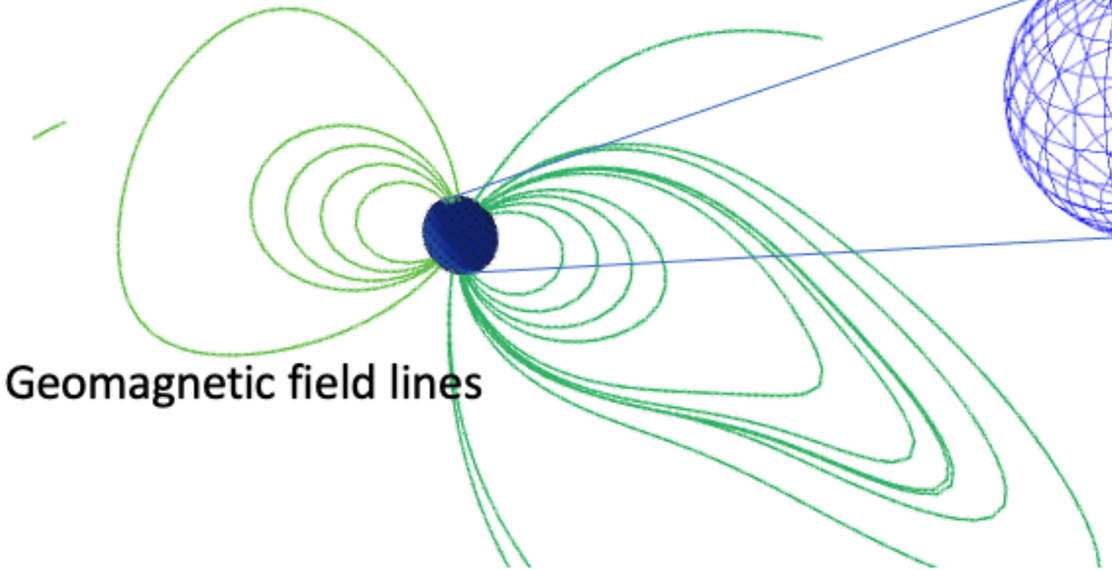

Geomagnetic field lines

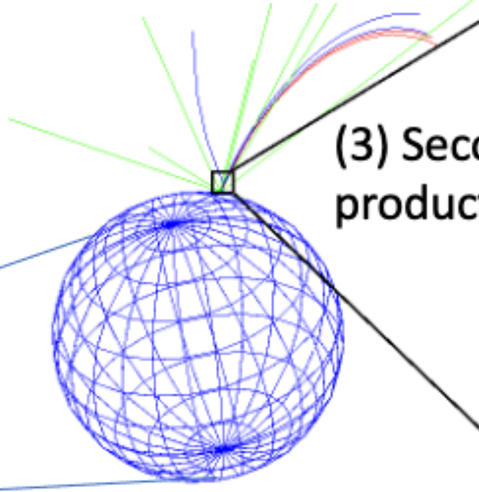

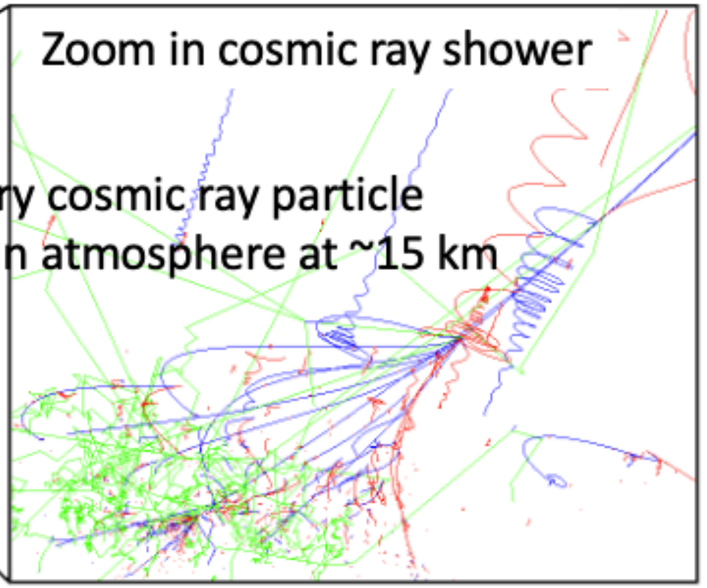

(3) Secondary cosmic ray particle production in atmosphere at ~15 km

These ionizing particles are regarded as health hazards for flight crew

(4) Most particles reaching to the surface of earth are muon particles together with a few percent of neutrons. By measuring muon flux variation around the world allows us to derive the state of space weather and atmospheric profile in real-time.

Figure 4.

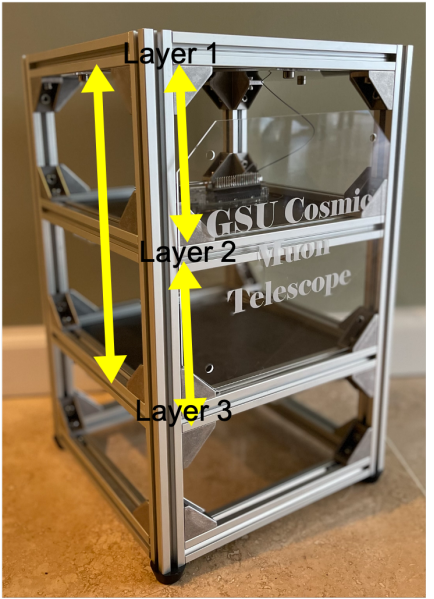

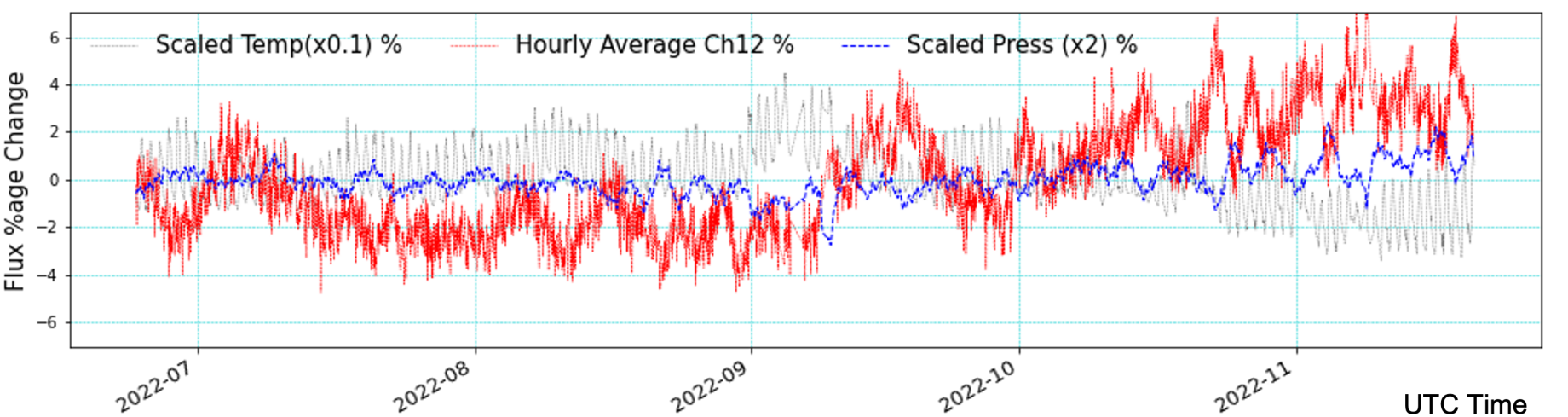

[Note: layer 1 & 2 distance = layer 2 & 3 distance. The average of coincidence counts between layer 1 & 2 is equal to the layer 2 & 3, which serves as a diagnostic tool of the detector performance.]

Figure 6.

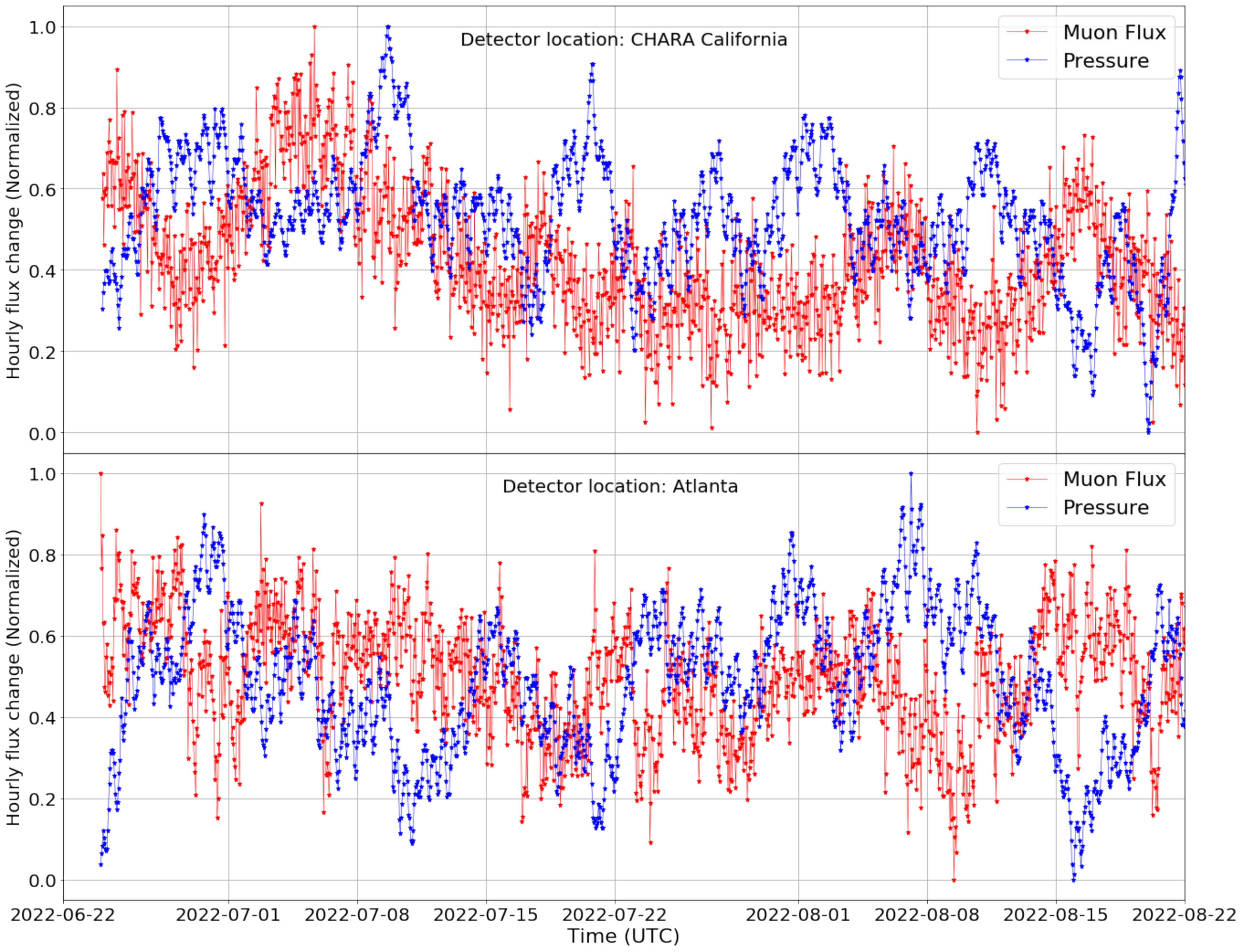
Detector location: CHARA California
Muon Flux
Pressure
Hourly flux change (Normalized)
1.0
0.8
0.6
0.4
0.2
0.0
Detector location: Atlanta
Muon Flux
Pressure
Hourly flux change (Normalized)
1.0
0.8
0.6
0.4
0.2
0.0
2022-06-22
2022-07-01
2022-07-08
2022-07-15
2022-07-22
2022-08-01
2022-08-08
2022-08-15
2022-08-22
Time (UTC)

Figure 3.

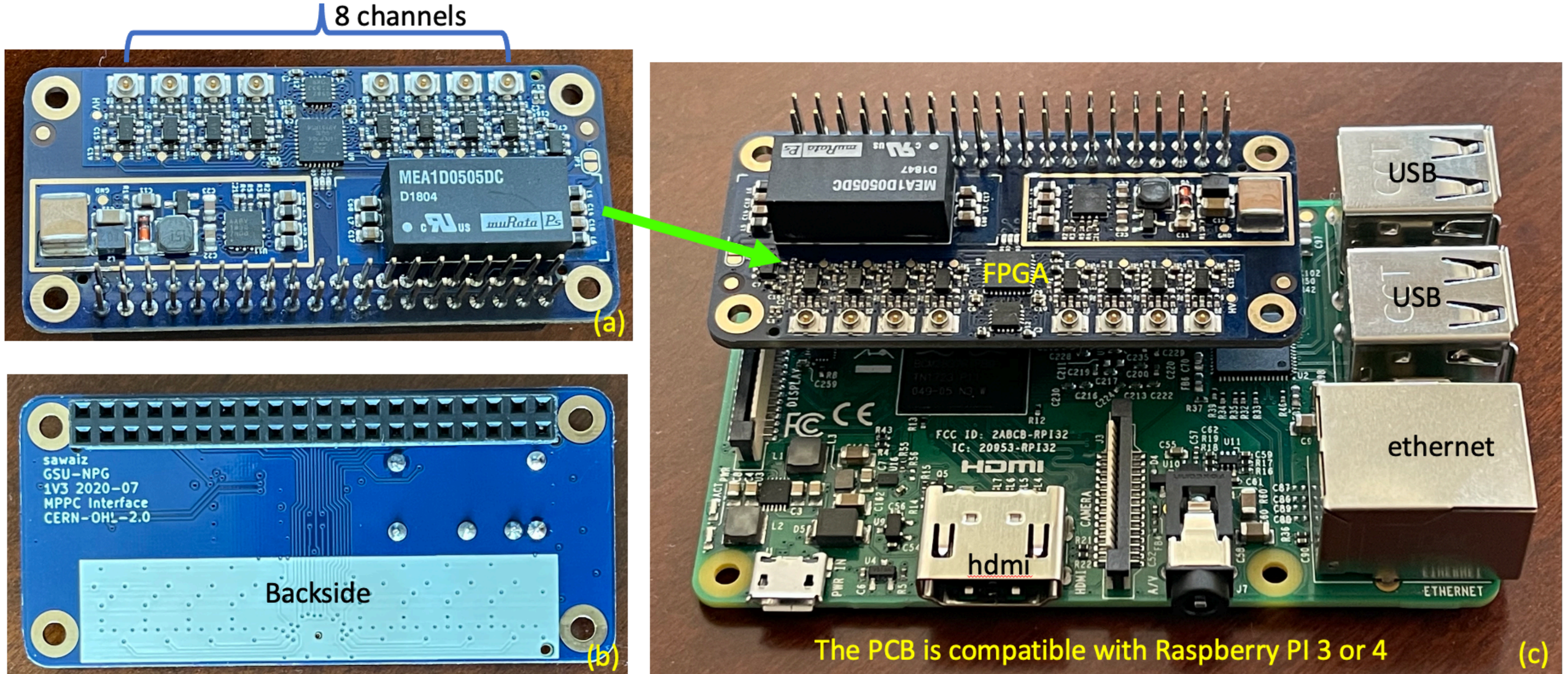
8 channels
MEA1D0505DC
D1804
muRata
(a)
sawaiz
GSU-NPG
1V3 2020-07
MPPC Interface
CERN-OHL-2.0
Backside
(b)
MEA1D0505DC
FPGA
USB
USB
ethernet
FCC ID: 2ABCB-RPI32
IC: 20953-RPI32
HDMI
hdmi
ETHERNET
The PCB is compatible with Raspberry PI 3 or 4
(c)

Figure 2.

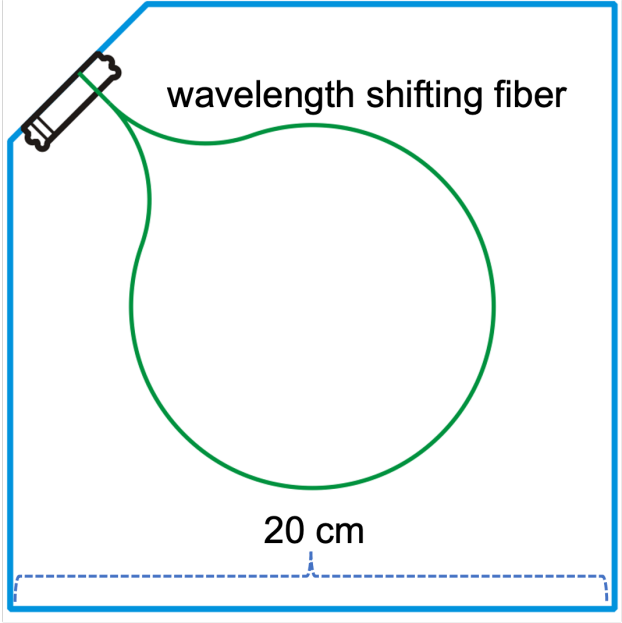
wavelength shifting fiber
20 cm

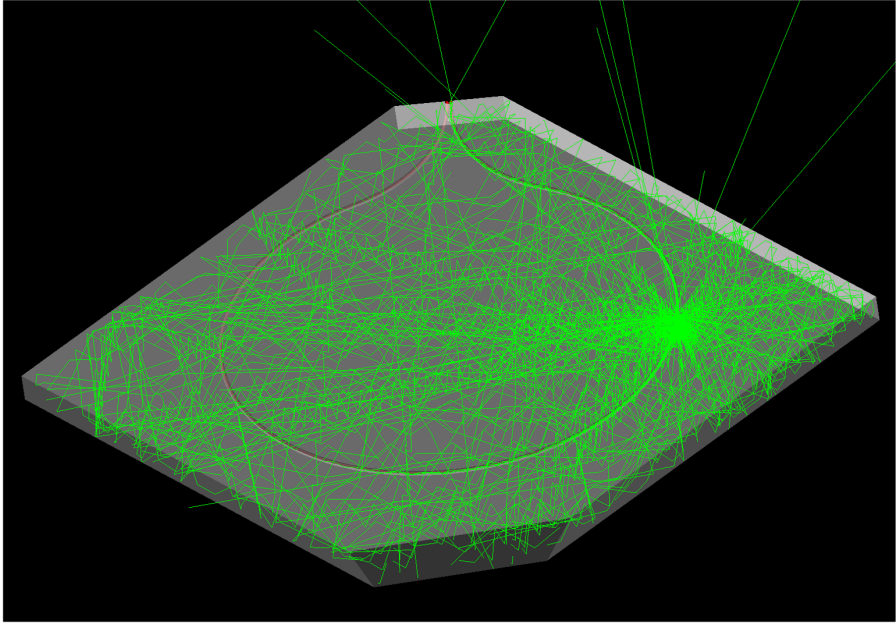

Figure 8.

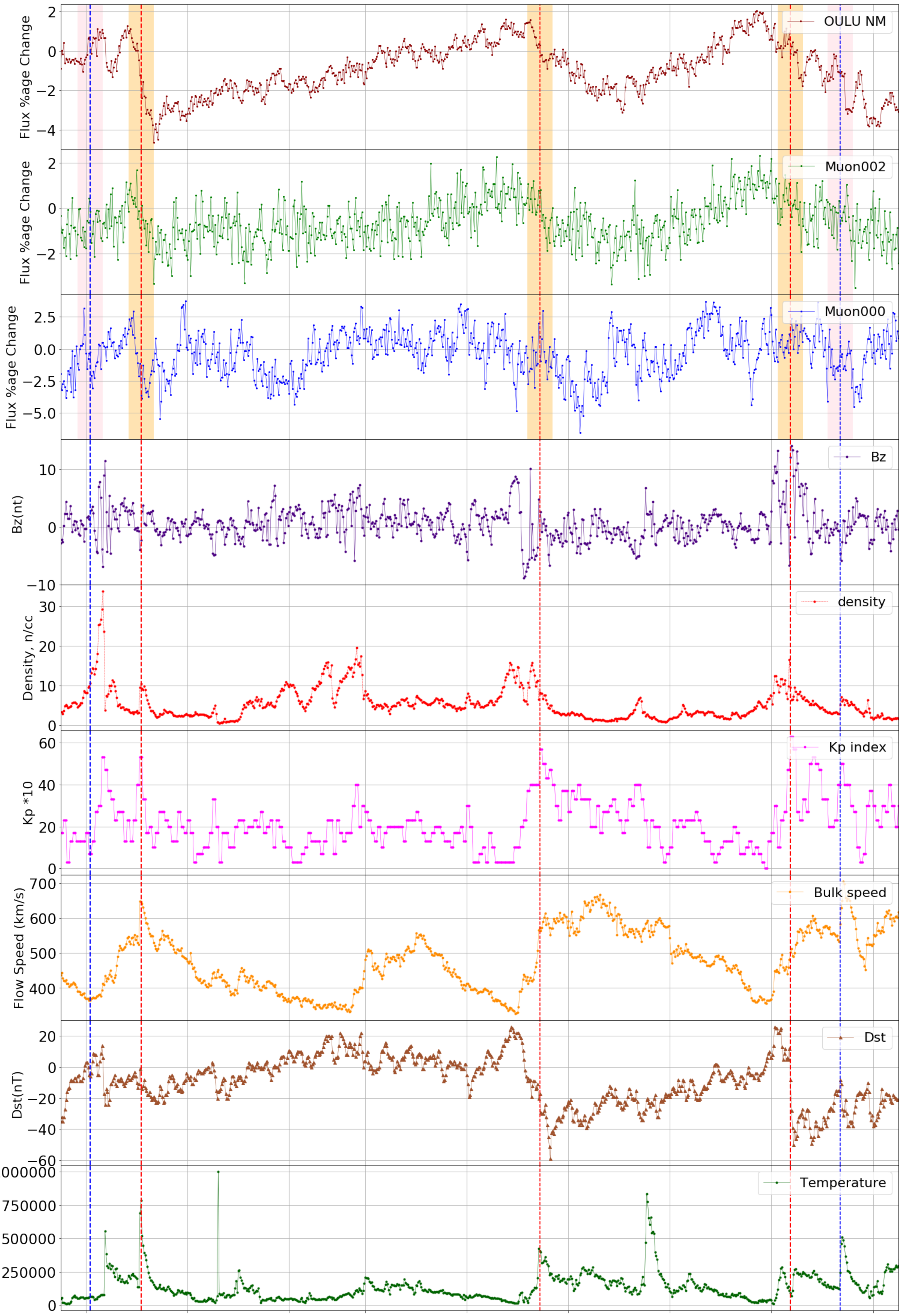
Flux %age Change
OULU NM
Muon002
Muon000
Bz(nt)
Bz
Density, n/cc
density
Kp *10
Kp index
Flow Speed (km/s)
Bulk speed
Dst(nT)
Dst
Temperature, K
Temperature
2022-07-21
2022-07-25
2022-07-29
2022-08-01
2022-08-05
2022-08-09
2022-08-13
2022-08-17
2022-08-21
Time (UTC)

Muon Flux Variation in Real-time and its Correlation with Space Weather Activity

A. Mubashir[1], A. Ashok[2], A.G. Bourgeois[2], Y.T. Chien[1], M. Connors[1], E. Potdevin[1], X. He[1], P. Martens[1], A. Mikler[2], A.G.U. Perera[1], V. Sadykov[1], M. Sarsour[1], D. Sharma[1], C. Tiwari[2,3]

[1]Department of Physics and Astronomy, Georgia State University
[2]Department of Computer Science, Georgia State University
[3]Department of Geosciences, Georgia State University

Corresponding author: X. He, xhe@gsu.edu

Abstract

We present a comparison of the measured cosmic ray (CR) muon fluxes from two identical detectors at different geolocations and their sensitivity to space weather events in real time. The first detector is installed at Mount Wilson Observatory, CA, USA (geomagnetic cutoff rigidity Rc $\sim$ 4.88 GV), and the second detector is running on the downtown campus of Georgia State University in Atlanta, GA, USA (Rc $\sim$3.65 GV). The variation of the detected muon fluxes is compared to the changes of the interplanetary solar wind parameters at L1 Lagrange point and geomagnetic indexes. We have also investigated the muon flux behavior during major interplanetary shock events and geomagnetic disturbances. To validate the interpretation of the measured muon signals, the muon fluxes are compared to the neutron flux measurement from the Oulu neutron monitor (NM) in northern Finland (Rc $\sim$0.8 GV). The results of this analysis show that the cosmic ray flux percentage changes from all stations are significantly correlated with each other and with solar wind parameters at L1, and the decreases of the muon fluxes can sometimes be observed several hours ahead of the onsets of the interplanetary shock arrivals at L1 and geomagnetic disturbances. Although this is yet an initial effort of building a global network of cosmic ray muon detectors for monitoring the space and earth weather in real time, the study provides evidence that muon network detection efficiency can be a diagnostic and forecasting tool for geomagnetic storms hours before they hit the Earth.

Key Points:

- A global network of portable muon detectors is under development for monitoring the dynamic changes of the space and terrestrial weather
- A comparison of the measured cosmic ray muon fluxes from two identical detectors at different geolocations in real-time is carried out
- A correlation study between the muon data and the neutron measurement at Oulu cosmic ray station in Finland is presented in this paper

Plain Language Summary

A pair of identical, low-cost, and portable cosmic ray muon detectors is set up over 3,500 km apart for an exploratory study of monitoring the space and terrestrial weather in real time at global scale. One detector is installed on Mount Wilson, California and the other is in downtown Atlanta, Georgia. To validate the interpretation of the measured muon signals, the muon fluxes are compared to the well-known neutron flux measurement from the Oulu neutron station in Finland. The results of this analysis show that the cosmic ray flux percentage changes from all stations are significantly correlated with each other and with the space weather activities. Although this is yet an initial effort of building a global network of cosmic ray muon detectors for monitoring the space and earth weather in real time, the study provides evidence that muon network detection efficiency can be a diagnostic and forecasting tool for geomagnetic storms hours before they hit the Earth.

1 Introduction

The interaction between the interplanetary space plasmas and the Earth's magnetosphere has vital importance in the context of space weather forecasting. The interplanetary space which is filled with the solar wind with frozen-in magnetic fields and cosmic ray (CR) particles is highly affected by solar magnetic activity which ultimately causes

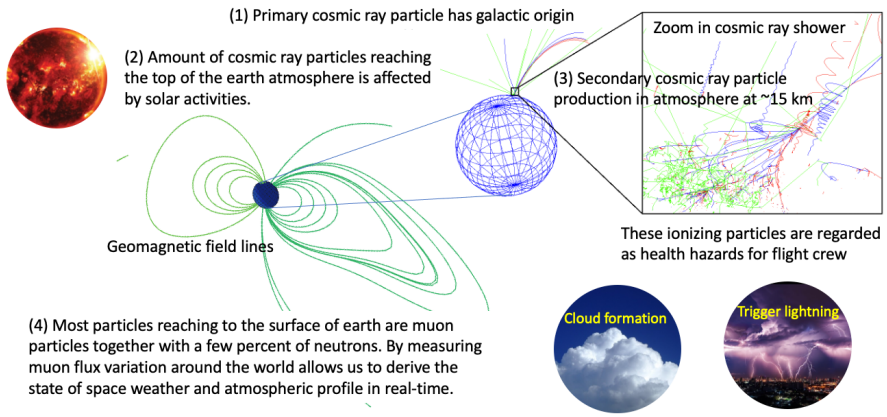

Figure 1. Cosmic ray interactions and propagation from deep in space, in the solar system, through the Earth's atmosphere, and to the surface of the Earth.

cosmic rays flux modulations in space and on Earth (Gleeson & Axford, 1968; Kojima et al., 2015). High-energy particles produced during the solar transient activities (so-called *solar energetic particles*, i.e. SEPs, Reames, 2021) as well as from outside the solar system (so-called primary *cosmic ray particles*) collide with nuclei of Earth's atmospheric molecules and produce secondary cosmic ray shower particles typically in a few kilometers above commercial airplane flying altitude. The most abundant particles reaching sea level are muons (about 80%, Zyla et al., 2020) together with a few percent of neutrons and electrons (ignoring neutrino particles which are irrelevant for this study). The solar activity, the state of the interplanetary space, and the Earth's magnetosphere and atmosphere are collectively responsible for the intensity of secondary cosmic ray particles being detected by ground-based cosmic ray detectors. Figure 1 highlights the four major processes of cosmic ray interaction and propagation.

Correlation studies between the cosmic ray flux and solar activity parameters (Munakata et al., 2000; Firoz et al., 2010; Dvornikov et al., 1988; Maghrabi et al., 2021) reveal that disturbances in the solar wind and shocks from the powerful solar transient events (flares, coronal mass ejections, and acceleration of solar energetic particles) may result in geomagnetic activity and cosmic ray modulation. Two main phenomena responsible for the modulation of the flux rate of cosmic rays incident on the Earth's upper atmosphere are the disturbances in the solar wind and the Earth's magnetic field (Firoz et al., 2010; Kudela et al., 1993). This modulation of cosmic rays can be analyzed by the peaks and valleys in their time series detected by ground-based particle detectors (Shrivastava & Jaiswal, 2003).

Solar wind modulates the incoming CR flux through diffusion, drift processes and adiabatic cooling (Parker, 1958). Changes in solar wind cause the magnetosphere to react, resulting in variations of the geomagnetic activity indices. The ring current strength and the related disturbance storm time are characterized using the Dst index, and the global variations of the horizontal magnetic fields measured at the Earth's surface are described using the Kp and Ap indexes (Cane & Richardson, 2003; Mishra & Mishra, 2018). Coronal mass ejections (CME) are large clouds of plasma with frozen in magnetic fields which can cause strong variations in the interplanetary magnetic field. Consequently, Earth's magnetic field may respond strongly to the CME passing through the Earth's orbit and interacting with the Earth's magnetosphere (Storini, 1990). At least 86 percent of the cosmic ray decreases observed by ground-based neutron monitors during the past 30 years are attributed to CME-driven geomagnetic storms (Cane & Richardson,

2003). Therefore the changes in the cosmic ray muon and neutron fluxes carry essential information about geomagnetic disturbances, solar eruptive events, and the solar wind, and may be used for the development of diagnostics and forecasting tools.

Knowledge of short-term cosmic ray modulation on a large scale is of great importance because of its correlation with various solar, interplanetary, and geophysical parameters (Sabbah, 2000). The key challenge in space and earth weather monitoring on a global scale using cosmic rays is to develop efficient, low-cost, and portable detectors that can provide accurate correlations between cosmic ray flux variations and the changes in solar activity and the atmospheric properties. Such a state-of-the-art portable muon particle detector has been developed by the Nuclear Physics Group at Georgia State University (GSU, He et al., 2021). An interdisciplinary team at GSU has successfully deployed its first remotely-installed cosmic ray muon detector (to be referred to as Muon002) on Mt Wilson, CA on June 7, 2022. The site is the home of the CHARA Array, a flagship project of GSU's Center for High Angular Resolution Astronomy (CHARA). This marks the beginning of a long-term effort by the team for building a global network of cosmic ray muon detectors for monitoring space and terrestrial weather. This network could be significant for predicting geomagnetic storms several hours early as studies reveal that ground based muon detectors via cosmic ray anisotropies can detect Earth-directed CMEs and interplanetary shock waves earlier than neutron monitors (Munakata et al., 2000; Jansen et al., 2001). The measurements by the identical muon detector installed at the GSU campus in downtown Atlanta (to be referred to as Muon000) provides a possibility to analyze the simultaneous response of both detectors to global magnetospheric disturbances and solar events.

The objective of this study is to investigate the short-term correlation of the cosmic ray muon and neutron flux variation with solar and geomagnetic activity. In particular, we report the first results of analyzing the time series of cosmic ray muon fluxes recorded by Muon000 and Muon002. The focus of this paper is to explore the sensitivity of the muon flux variations measured by these two detectors in connection with recent space weather activity. The paper is divided into four sections. Section 2 presents the detector setup, data sources, and the associated data analysis details. The discussion of results is presented in Section 3 while Section 4 concludes the paper.

2 Detector Setup and Dataset Sourses

2.1 Cosmic ray muon detector design and configuration

The design goals of our cosmic ray muon detector include that (a) it should be at a low cost and with portability in order to install affordable and identical detectors around the world, (b) it should support remote data access and maintenance, and (c) the scintillator tile should be large enough to be sensitive to the changes of local meteorological parameters and the space weather. The key components of the detectors include three plastic scintillator tiles (20cm x 20cm x 1cm) embedded with wavelength shifting fibers as shown in Fig. 2. The purpose of using wavelength shifting fiber is to transport photons generated by a passing muon particle to a silicon photomultiplier (call SiPM) which is mounted at the cut corner of the tile. Extensive simulation based on the GEANT4 software package (Allison et al., 2016) has been performed to validate the design for light collection uniformity and efficiency.

The detector signal readout is achieved by using a dedicated PCB mounted to a low cost computer (Raspberry PI) readout, as shown in Fig. 3. The total cost of the readout hardware (including the PCB and the Raspberry PI) is less than 250 US dollars which fulfill our design requirements. The Raspberry PI computer running Linux OS provides the functionality of configuring, data taking, and remote access.

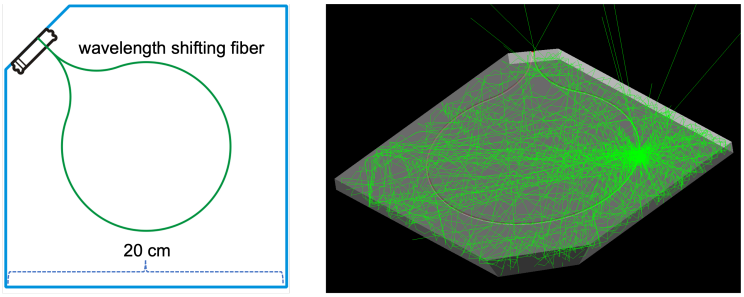

Figure 2. Scintillator design of cosmic ray muon detector: (left) CAD model of scintillating tile with an embedded wavelength shifting fiber; (right) a GEANT4 based simulated event display of scintillating photon collection.

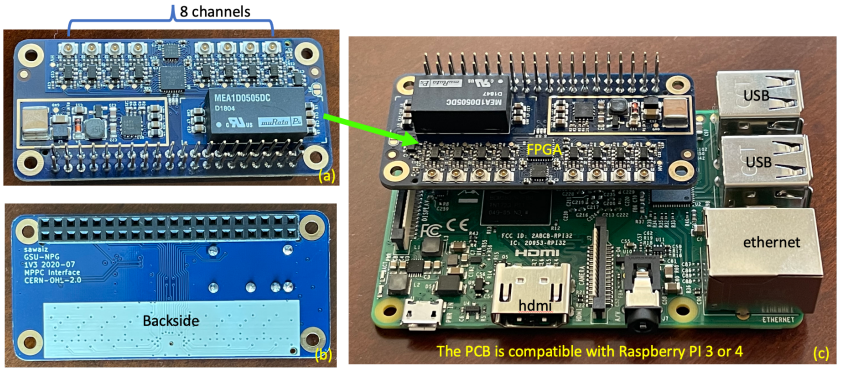

Figure 3. Muon detector signal readout design: (a) front PCB with 8-channel connections at the top; (b) backside of the PCB; (c) A Raspberry PI 3 with a PCB mounted to its GPIO pins.

In our baseline design of the cosmic muon detector, the three scintillating tiles are supported by an extruded aluminum frame as shown in Fig. 4. The separation distance between layers 1 and 2 is equal to the distance between layers 2 and 3, which allows us to make a quick check of the detector performance since one is expecting equal average coincidence counts between layers 1 & 2 and layers 2 & 3. The plot in Fig. 4 shows the time series of hourly muon flux (i.e., coincidence between layers 1 and 2 in red) percent change in recent months. Also shown in the plot are the scaled percent changes of the local atmospheric pressure and temperature at ground level, which clearly demonstrate the well-known and classic trend of the correlation between muon flux and pressure.

In this exploratory study, we focus on analyzing data recorded from two detectors. One of the detectors running on the GSU campus (to be referred to as Muon000) is installed on the 4th floor of a 5-floor building. Its GPS coordinate is 33° 44′ 56.38″ N and 84°23′16.74″ W with cutoff rigidity $R_c \sim 3.65$ GV. The second detector was installed at the CHARA site on Mount Wilson on June 7, 2022 (to be referred to as Muon002). Its GPS position is 34° 13′ 15.31″ N and -118° 03′ 25.15″ W with an elevation of 1,740 m and cutoff rigidity $R_c \sim 4.88$ GV, as shown in Fig. 5

Cosmic ray flux is recorded every minute by both detectors and hourly data is then used in the present study. Hourly pressure data for the considered period is downloaded from automated weather observations provided by Iowa State University[1] used for the

[1] `https://mesonet.agron.iastate.edu/`

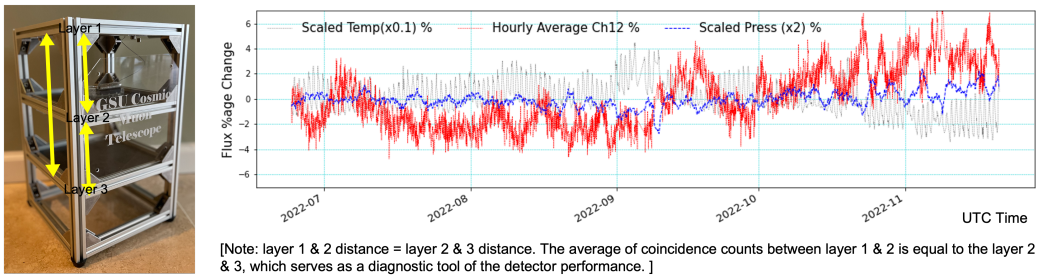

Figure 4. The baseline muon detector setup is shown on left with the adjacent scintillator layers 12.7 cm apart. The coincidence counts between layers 1 and 2, 2 and 3, and 1 and 3 are recorded in every minute. The plot on right shows a time-series of the percentage change of the hourly counts between layer 1 and 2 together with the precentages of ground level pressure and temperature.

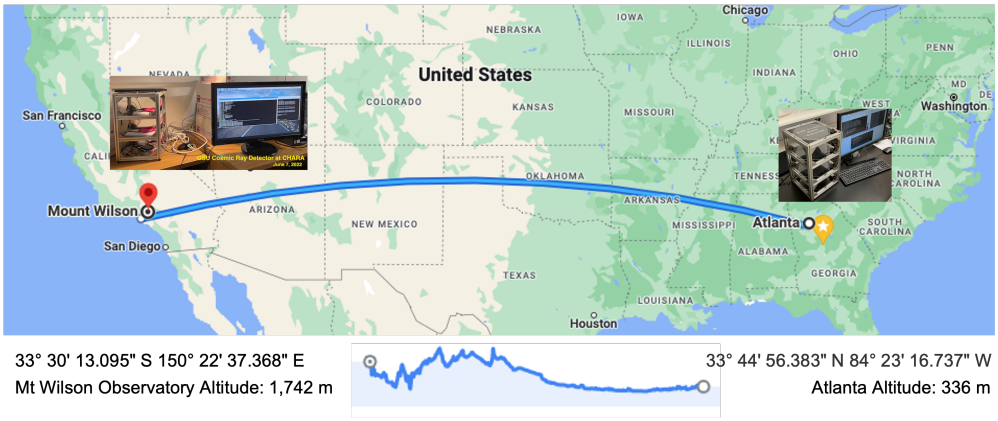

Figure 5. Cosmic ray muon detectors included in this study. The two detectors are ∼3,500 km apart. The altitude of the detector on Mount Wilson is 1,742m and a higher muon flux is recorded in this detector in comparison with the recorded muon flux in Atlanta.

pressure correction of muon counts. For comparison of muon flux vs neutron flux, another data set used in this study is of neutron monitor (NM) counts from Oulu (65.05°N, 25.47°E) which is one of the well known and stable neutron detector stations actively measuring neutron flux on the ground level. Oulu data is publicly available online[2].

2.2 Solar activity and wind parameters

The solar wind and geomagnetic parameters used in this study are solar wind plasma speed, density, B_z component of Interplanetary Magnetic Field (IMF), kinetic energy, planetary K_p index, and disturbance storm time Dst index in Geocentric Solar Magnetospheric (GSM) coordinate system. Data deduction is done from the Low Resolution OMNI (LRO) data set of NASA's catalog[3]. Interplanetary shocks information for the considered period of study is taken from the Database Of Notifications, Knowledge, Information developed at NASA Community Coordinated Modeling Center (DONKI at

[2] https://cosmicrays.oulu.fi/
[3] https://omniweb.gsfc.nasa.gov/html/ow_data.html

CCMC[4]) and a news archive of Space Weather Prediction Center at National Oceanic and Atmospheric Administration (SWPC NOAA[5]).

3 Data Analysis

To quantify the cosmic ray flux modulations, it is important to have knowledge of variations in solar and interplanetary parameters (Belov et al., 2005). The measured cosmic ray flux at ground level depends on the intensity of cosmic ray flux above the Earth's atmosphere and the atmospheric profile at the detector location. The atmospheric thickness is directly associated with the local pressure measurements at the detector location (Kobelev et al., 2011). In order to explore the sensitivity to space weather-related processes and to represent the galactic cosmic ray intensities, calculation of barometric coefficient and applying pressure correction on data is a prerequisite (Dorman, 2004; Koldobskiy et al., 2022).

3.1 Barometric effect on muon flux and pressure correction

The very first step of the data analysis is to look at the time series of the recorded cosmic ray counts and to identify the events of interest with large decrease of the counts. Both Muon000 and Muon002 record muon counts in one-minute intervals. We sum the minute-count into hourly counts and then calculate the percentage changes of the hourly counts from the mean. Figure 6 shows the normalized percentage change of the hourly muon counts for both detectors together with the hourly ground level pressure, at the location of detector, over a time period ranging from June 24 to August 22, 2022. The normalization is done by scaling the percentage change to the range of 0 to 1 using the python built-in MinMaxScalar function.

As it is shown in Fig. 6, the muon fluxes from both detectors are in anti-correlation with the observed atmospheric pressure. We remove the effect of pressure variation on muon flux using equation 1 (Kobelev et al., 2011; Dorman, 2004; Koldobskiy et al., 2022):

$$N_{i,corr} = N_i e^{-\beta(P_i - P_o)} \tag{1}$$

Here N_i and $N_{i,corr}$ correspond to the recorded hourly and the pressure corrected muon counts respectively. P_i is the downloaded hourly pressure and P_o represents the average pressure during the time period of this study. The barometric coefficient, β, is obtained by fitting a linear regression model between $ln(\frac{N_i}{N_o})$ and $(P_i - P_o)$. The β values obtained from the fit are -0.2%/mb and -0.06%/mb for Muon000 and Muon002, respectively. These values agree within the systematics to the previously reported β-values (-0.114 %/mb to $-$ 0.18%/mb) obtained from similar muons analyses reported in (De Mendonça et al., 2013; Berkova et al., 2011; Dmitrieva et al., 2013).

It is well known that there is a seasonal variation of the muon flux, which is related to the expansion of the atmosphere to a higher altitude in summer period. This study only covers a two-month period in summer of 2022, we simply ignore the temperature effects for the current analysis.

3.2 Cross comparison of cosmic ray detector data

As already stated in the introduction, the main objective of this study is to investigate the short-term correlation of the cosmic ray muon flux variations in a detector network with solar and geomagnetic activity. Figure 7 shows the pressure-corrected percentage changes of the hourly muon counts from Muon000 and Muon002 in UTC time, plot-

[4] `https://kauai.ccmc.gsfc.nasa.gov/DONKI/search/`
[5] `https://www.swpc.noaa.gov/news-archive`

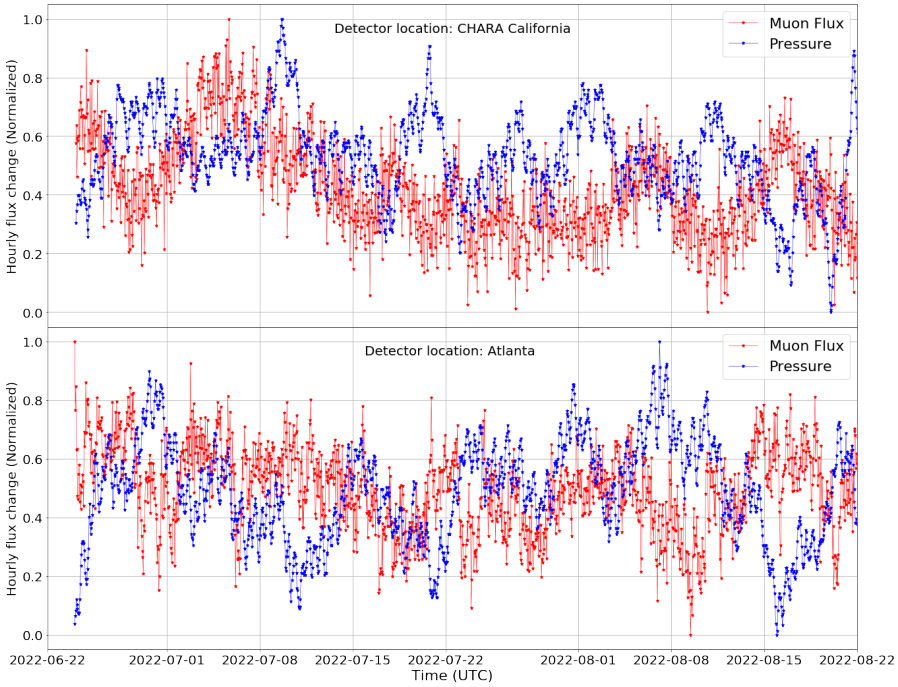

Figure 6. Normalized hourly muon flux percentage change (in red) time series of Muon002 and Muon000 overlaid with ground level pressure (in blue). A clear trend of the well-known anti-correlation between the muon flux and the local ground level pressure is seen for both detectors.

ted together with the pressure-corrected percentage change of the hourly neutron counts for comparison, the data for which is obtained from the Oulu neutron station .

In the current reported time period of two months, the general trend of dips and peaks in the time series of neutron counts is in strong visual correlation with the flux percentage changes in both muon detectors. The Pearson correlation coefficient found between Oulu vs Muon002, Oulu vs Muon000, and Muon002 vs Muon000 is 0.70, 0.20, and 0.28 respectively. The differences in the time series among these detectors are attributed to the detector locations with different geomagnetic cut-offs and altitude. For Oulu NM and Muon002, the percentage flux variability ranges around ±4 percent, while for Muon000 percentage flux variability ranges around ±6 percent. It is evident from Fig. 7 that for some specific time period, all detectors showed continuous decreasing flux percentage change corresponding to the lower number of counts. The decreasing trend in form of negative peaks can be related to space weather activity events which are explained in the next section.

3.3 Sensitivity of muon flux variation to space weather activity

Solar activity causes variation in the cosmic ray flux that can have different magnitudes and different time scales based on the detector geolocation (Maghrabi et al., 2021). The evolution of the cosmic ray fluxes in the vicinity of the geomagnetic storm times is presented in more details in Fig. 8. Besides these fluxes, we plot the time moments corresponding to the geomagnetic storms and interplanetary shocks according to the DONKI CCMC. We also tracked the news archive of SWPC NOAA for verifying the presence of these space weather events. Although DONKI contains only two geomagnetic storms in August 2022 (starting at 2022-08-07T21:00, and two subsequent storms at 2022-08-17T18:00 and 2022-08-18T00:00), we mark one more storm point at 2022-07-23T03:59

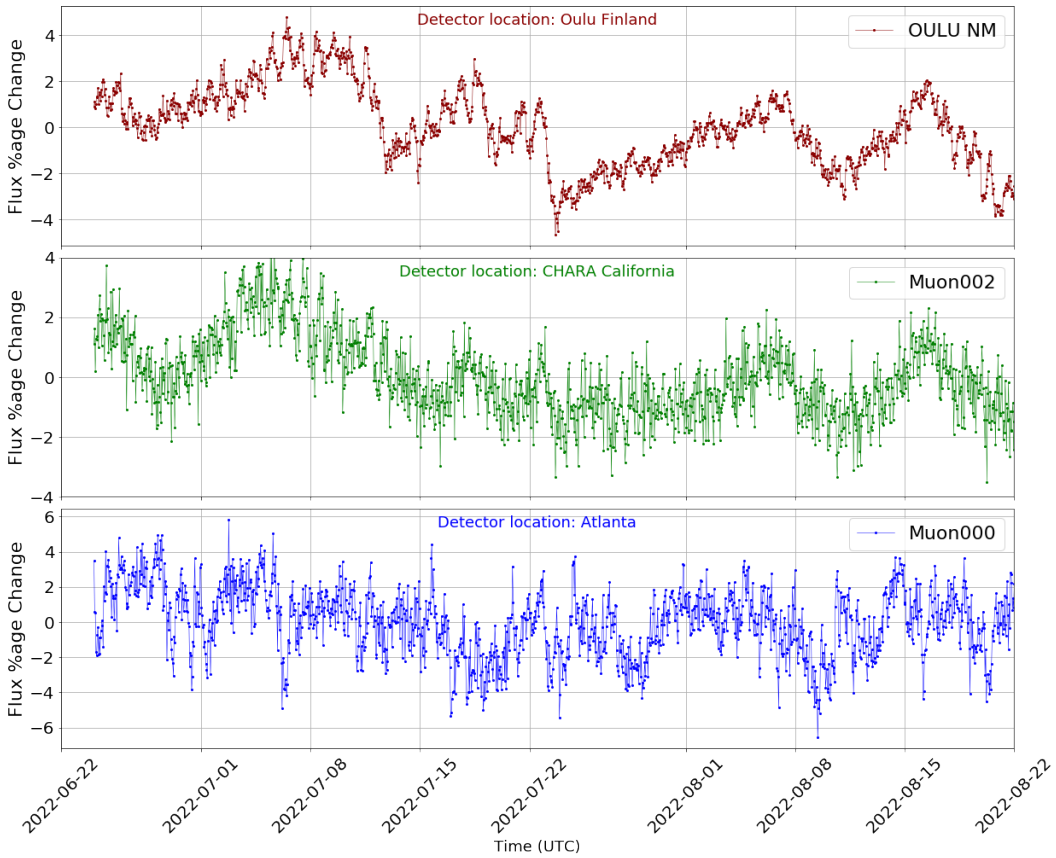

Figure 7. Comparative analysis of cosmic ray flux time series from the Oulu neutron station (top), Muon002 (middle) and Muon000 (bottom) after the atmospheric pressure correction.

which corresponds to a high-Kp level as shown in Fig. 8 and was reported[6] by SWPC NOAA. One of the prominent features often seen in both detectors before geomagnetic storm onsets is the steady decrease in the pressure-corrected muon counts sometimes several hours before the storms (in Fig. 8 yellow segmented bars show ±12 hours to the storms, and two pinks bars mark the same intervals for ICMEs not related to the storm activities). The two minor geomagnetic storms (G1) and one minor to major (G1-G3) geomagnetic storm associated with Kp >5, strong Dst depression and negative Bz peaks show a drastic shift of percentage flux change 12 hours prior to the closest approach of the geomagnetic storms.

To quantify the level of sensitivity, we estimate the flux changing rate (i.e., slope) at each of the geomagnetic storms with three time-interval in hours: ±12, ±6, and ±3. The flux change rates during these events for different time intervals are summarized in Table 1. The presence of the preceding Interplanetary Coronal Mass Ejection (ICME) shocks observed at L1 Lagrange Point by the Deep Space Climate Observatory (DSCOVR) and the solar drivers of the ICME shocks (coronal mass ejections, CMEs, or high-speed streams, HSS) is indicated in the footnotes of the table. As it is seen in Table 1, the computed slope values are the largest for the first geomagnetic storm for all three detectors of ±3-hour, ±6-hour and ±12-hour interval. Similar dependence can be seen for other events but with lesser steep slopes. After the occurrence of each geomagnetic storm, per-

[6] `https://www.swpc.noaa.gov/news/g1-minor-geomagnetic-storming-observed-23-july`

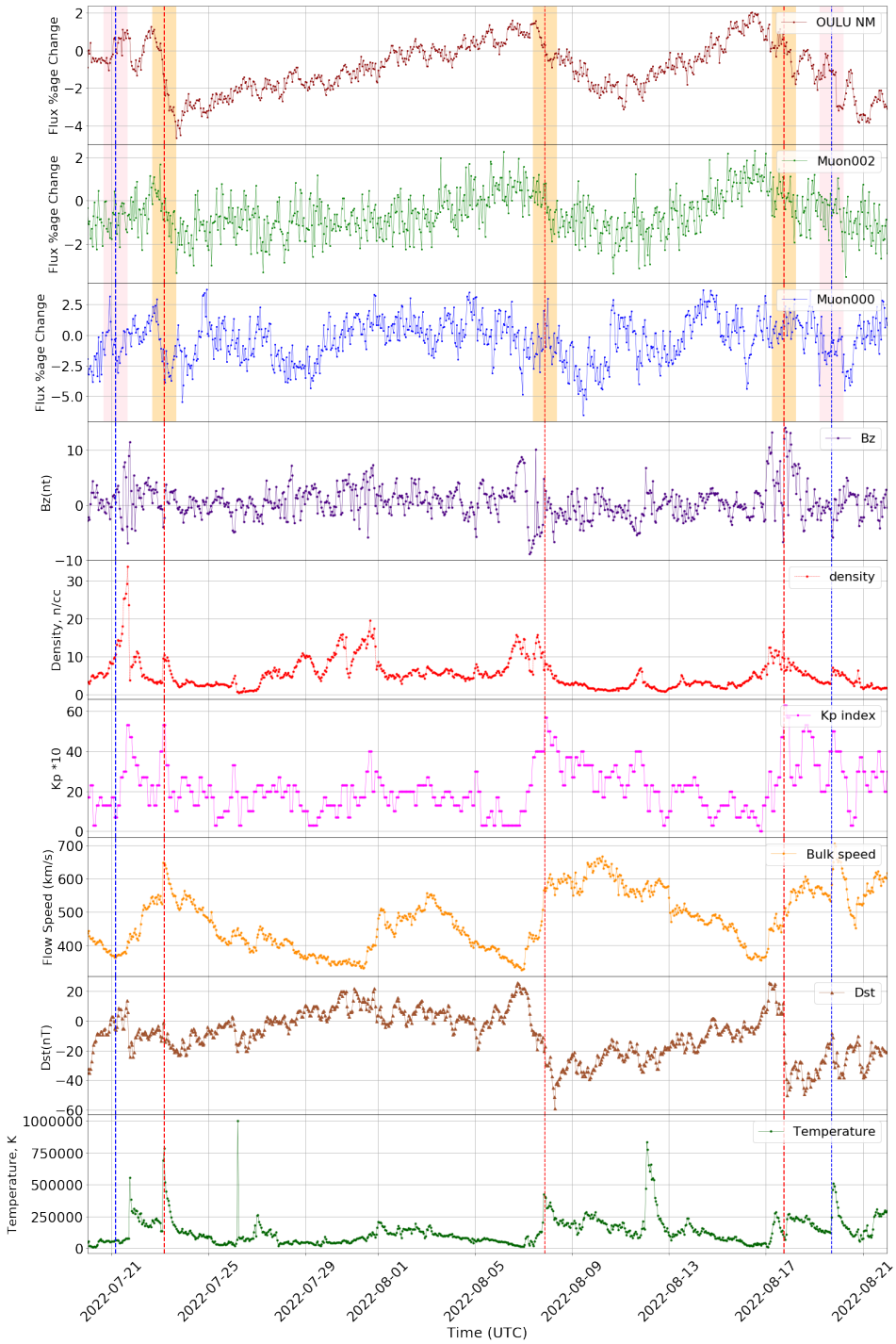

Figure 8. Time series of pressure-corrected cosmic ray flux percentage changes and the space parameters from 2022-07-20T00:00 UT to 2022-08-22T00:00 UT. The vertical red dashed line within the shaded bars marks the times of the geomagnetic storm at 2022-07-23T03:59, 2022-08-7T21:00, and 2022-08-17T18:00 while vertical blue lines mark the ICME shocks (IP) on 2022-07-21T03:54 and 2022-08-19T17:02

Table 1. Summary of the transient rates of muon and neutron flux percentage change at the times of three geomagnetic storms. The rates are calculated in three time windows: ±12 hours, ±6 hours, and ±3 hours with respect to the geomagnetic storm times.

	Slope in ±12 hr (%/h)			Slope in ±6 hr (%/h)			Slope in ±3 hr (%/h)		
	GS1[a]	GS2[b]	GS3[c]	GS1	GS2	GS3	GS1	GS2	GS3
Muon000	-0.27	0.03	0.20	-0.68	-0.13	0.42	-0.41	1.4	-0.20
Muon002	-0.26	-0.03	-0.007	-0.18	-0.41	0.13	-0.14	-0.03	-0.06
Oulu	-0.45	-0.14	-0.16	-0.50	-0.24	-0.15	-0.77	-0.27	-0.19

[a] Geomagnetic Storm 1 (2022-07-23 03:59:00, G1). Preceding events: 2022-07-23 02:28:00 (IP), 2022-07-21 01:36:00 (CME).

[b] Geomagnetic Storm 2 (2022-08-07 21:00:00, G1). Preceding events: 2022-08-07 00:45:00 (IP, HSS).

[c] Geomagnetic Storm 3 (2022-08-17 18:00:00, G1-3). Preceding events: 2022-08-17 02:14:00 (IP), 2022-08-17 02:14:00 (CME).

centage flux change had its minimum value in the next 6 to 12 hours which is followed by the recovery phase in time. During the third minor to major (G1 to G3) storm, there were two days of geomagnetic disturbances caused by the multiple coronal mass ejections near Earth starting on August 14, 2022. The continuous decrease of flux seen from August 17 to 19 could be due to this effect.

Along with the flux behavior of muon detectors at GSU and CHARA, and of neutron monitor in Oulu, Fig. 8 also illustrates the variations of the solar wind and geomagnetic activity parameters during the time period of July 8 to August 22, 2022. One notices that all the solar wind and geomagnetic activity parameters (total magnetic fields, densities, flow speeds, plasma temperatures) start to become enhanced prior to the geomagnetic storms / interplanetary shock times. B_z and Dst also become negative, indicating conditions favorable for the geomagnetic storm development. The Kp indexes were strongly elevated during the events as well. DONKI indicates that all these three events have associated interplanetary shock detected at the L1 point (on 2022-07-23T02:28, 2022-08-07T00:45, and 2022-08-17T02:14, correspondingly, indicated in the footnotes of Table 1). A possible interpretation of the overall decrease in fluxes of muon and neutron detectors is their relation to the Forbush decrease effect (Janvier et al., 2021), a result of an interplanetary CME passing by the Earth and deflecting an additional fraction of cosmic rays by an embedded magnetic field. This may indicate the sensitivity of the fluxes measured by muon detectors (both Muon000 and Muon002) to space weather events.

For this short-term analysis, Pearson correlation coefficients between the flux variations of all detectors and the considered solar parameters were calculated, which were found to be anti-correlated with flow rate, plasma temperature, and Kp index, whereas the variations were correlated with Dst and density. Among the two muon detectors, Muon 002 was found to be more sensitive with correlation coefficients of -0.27 and -0.17 between the muon flux change and, the flow speed and temperature (K), respectively. These values are close to the Oulu NM values which were -0.37 and -0.19 respectively. Also, a direct correlation between the muon flux and, the Dst and the density, was found with correlation coefficients of 0.20 and 0.17 respectively, while for Oulu NM the corresponding values were 0.34 and 0.35.

4 Summary and Outlook

In this paper, an exploratory study is carried out for assessing the feasibility and sensitivity of a global cosmic ray muon detector network for monitoring space weather activity. The results are based on the data recorded by a pair of identical detectors 3,500 km apart from June 24, 2022, to the end of August 2022. Our key findings are as follows:

1. Both muon monitor detectors installed at different locations/heights and corresponding to different geomagnetic cut-off rigidities (Rc $\sim$ 4.88 GV and Rc $\sim$3.65 GV for detectors in Mount Wilson, CA and Atlanta, GA, respectively) demonstrate similar patterns of their reaction to space weather events (decrease of fluxes before and during the geomagnetic storms, see Table 1). Muon fluxes are also correlated with the neutron monitor fluxes measured at Oulu station, at much lower geomagnetic cutoff rigidity (Rc $\sim$0.8 GV).
2. In many cases, muon fluxes show a decreasing trend several hours before the major geomagnetic storms and the trend continues during the storm period. A possible interpretation for these reductions is the effects of the interaction of cosmic rays with the ICMEs and their shock fronts, i.e. the Forbush decreases.
3. Muon fluxes measured in two detectors are correlated with each other (Pearson correlation coefficient of $r = 0.28$). The muon002 detector (installed at Mount Wilson) is found to correlate with the parameters of the interplanetary solar wind measured at L1 Lagrange point and the disturbance storm time index ($r = -0.27$, $r = -0.17$ and $r = 0.20$ with the solar wind speed, temperature, and Dst, respectively). These values are close to those found for neutron monitor at oulu station $r = -0.37$, $r = -0.19$, and $r = 0.34$ respectively. Muon002 also demonstrates a significantly higher correlation with the neutron monitor at Oulu station ($r = 0.7$) in comparison to Muon000 ($r = 0.2$).

It is evident that while reacting to space weather events, the muon detectors experience much stronger fluctuations of their signal. There are two possible reasons for that behavior. First, there is a strong coupling of the muon fluxes to the properties of the Earth's atmosphere which we find in our following works. As pointed out above, the detector on Mount Wilson (Muon002) demonstrates a much higher correlation with the Oulu neutron monitor than the detector installed in Atlanta (Muon000). Muon002 is installed in a higher altitude with respect to sea level (h=1740 m) than the detector in Atlanta and, therefore, it has less air mass above it and has less impact on the muon fluxes measured. A second possible reason is that the geomagnetic cutoff rigidities of muon detectors (Rc $\sim$ 4.88 GV and Rc $\sim$3.65 GV, respectively) are several times larger than of the neutron monitor at Oulu (Rc $\sim$0.8 GV) and, therefore, do not result in such a high sensitivity to space weather as for Oulu. Choosing future locations at higher altitudes of lower geomagnetic cutoff rigidities may help to confirm these possible reasons for signal volatility.

The sensitivity of the muon detectors to both the space and terrestrial weather properties represents, on one hand, a challenge to an interpretation of their signals and, on the other hand, an opportunity to build novel diagnostics and prediction capabilities. The affordability of the detector (the cost is slightly more than $\$1,000$), its portability and compact size, and low demands on maintenance (internet/WiFi and a standard power supply) make it an ideal instrument for the expansion to the full-scale network. In the future, we plan to expand the network of muon detectors and install them at different locations for monitoring both the space and terrestrial weather properties.

Open Research

The solar wind measurements onboard NASA's Deep Space Climate Observatory (DSCOVR) mission used in this study are openly accessible via the DSCOVR Space Weather Data Portal (`https://www.ngdc.noaa.gov/dscovr/portal/index.html#/`). The data from the Oulu neutron monitor are openly accessible via the Neutron Monitor Database (`https://www.nmdb.eu/`). The atmospheric pressure data from two ground weather stations at Atlanta Intl Airport (ATL) and Los Angeles Downtown (CQT) used for the pressure correction of muon monitors are openly accessible from the Iowa Environmental Mesonet (`https://mesonet.agron.iastate.edu/`). The space weather indexes (Kp and Dst) were obtained from the OMNIWeb database (`https://omniweb.gsfc.nasa.gov/form/dx1.html`). The raw and pressure-corrected muon detector counts from muon000 and muon002 detectors are publicly available at the Zenodo (`https://doi.org/10.5281/zenodo.7626767`).

Acknowledgments

The authors would like to acknowledge the support of the study under the GSU RISE program and thank the staff at CHARA for providing the space and computing network connection for data collection. VS acknowledges the NSF FDSS grant 1936361.

References

Allison, J., et al. (2016). Recent developments in geant4. *Nuclear Instruments and Methods in Physics Research Section A: Accelerators, Spectrometers, Detectors and Associated Equipment*, *835*, 186-225. Retrieved from `https://www.sciencedirect.com/science/article/pii/S0168900216306957` doi: https://doi.org/10.1016/j.nima.2016.06.125

Belov, A., Baisultanova, L., Eroshenko, E., Mavromichalaki, H., Yanke, V., Pchelkin, V., ... Mariatos, G. (2005). Magnetospheric effects in cosmic rays during the unique magnetic storm on november 2003. *Journal of Geophysical Research: Space Physics*, *110*(A9).

Berkova, M., Belov, A., Eroshenko, E., & Yanke, V. (2011). Temperature effect of the muon component and practical questions for considering it in real time. *Bulletin of the Russian Academy of Sciences: Physics*, *75*(6), 820–824.

Cane, H., & Richardson, I. (2003). Interplanetary coronal mass ejections in the near-earth solar wind during 1996–2002. *Journal of Geophysical Research: Space Physics*, *108*(A4).

De Mendonça, R., Raulin, J.-P., Echer, E., Makhmutov, V., & Fernandez, G. (2013). Analysis of atmospheric pressure and temperature effects on cosmic ray measurements. *Journal of Geophysical Research: Space Physics*, *118*(4), 1403–1409.

Dmitrieva, A., Astapov, I., Kovylyaeva, A., & Pankova, D. (2013). Temperature effect correction for muon flux at the earth surface: estimation of the accuracy of different methods. In *Journal of physics: Conference series* (Vol. 409, p. 012130).

Dorman, L. I. (2004). *Cosmic rays in the earth's atmosphere and underground* (Vol. 303). Springer Science & Business Media.

Dvornikov, V., Sdobnov, V., & Sergeev, A. (1988). Anomalous variations of cosmic rays in the 2-5 gv rigidity range and their relation to heliospheric disturbances. *Izvestiya Akademii Nauk SSSR, Seriya Fizicheskaya*, *52*(12), 2435–2437.

Firoz, K., Kumar, D., & Cho, K.-S. (2010). On the relationship of cosmic ray intensity with solar, interplanetary, and geophysical parameters. *Astrophysics and Space Science*, *325*(2), 185–193.

Gleeson, L. J., & Axford, W. (1968). The solar radial gradient of galactic cosmic rays. *Canadian Journal of Physics*, *46*(10), S937–S941.

He, X., Butler, C., Syed, S., Potdevin, E., Tarrant, P., Chen, N., & Wei, T. (2021). Development and production of modular cosmic ray telescopes.

Jansen, F., Munakata, K., Duldig, M., & Hippler, R. (2001). Muon detectors–the real-time, ground based forecast of geomagnetic storms in europe. In *Esa space weather workshop: Looking towards a european space weather programme.*

Janvier, M., Démoulin, P., Guo, J., Dasso, S., Regnault, F., Topsi-Moutesidou, S., ... Perri, B. (2021, December). The Two-step Forbush Decrease: A Tale of Two Substructures Modulating Galactic Cosmic Rays within Coronal Mass Ejections. *The Astrophysical Journal*, *922*(2), 216. doi: 10.3847/1538-4357/ac2b9b

Kobelev, P., Belov, A., Mavromichalaki, E., Gerontidou, M., & Yanke, V. (2011). Variations of barometric coefficients of the neutron component in the 22-23 cycles of solar activity. *Proc. 32nd ICRC*.

Kojima, H., Antia, H., Dugad, S., Gupta, S., Jagadeesan, P., Jain, A., ... others (2015). Dependence of cosmic ray intensity on variation of solar wind velocity measured by the grapes-3 experiment for space weather studies. *Physical Review D*, *91*(12), 121303.

Koldobskiy, S. A., Kähkönen, R., Hofer, B., Krivova, N. A., Kovaltsov, G. A., & Usoskin, I. G. (2022). Time lag between cosmic-ray and solar variability: Sunspot numbers and open solar magnetic flux. *Solar Physics*, *297*(3), 1–18.

Kudela, K., Slivka, M., Stehlik, M., & Geranios, A. (1993). Cosmic-ray fluctuations and interplanetary magnetic fields. *Astrophysics and space science*, *199*(1), 125–132.

Maghrabi, A., Aldosari, A., & Almutairi, M. (2021). Correlation analyses between solar activity parameters and cosmic ray muons between 2002 and 2012 at high cutoff rigidity. *Advances in Space Research*, *68*(7), 2941–2952.

Mishra, V., & Mishra, A. (2018). Long-term modulation of cosmic-ray intensity and correlation analysis using solar and heliospheric parameters. *Solar Physics*, *293*(10), 1–22.

Munakata, K., Bieber, J. W., Yasue, S.-i., Kato, C., Koyama, M., Akahane, S., ... Duldig, M. L. (2000). Precursors of geomagnetic storms observed by the muon detector network. *Journal of Geophysical Research: Space Physics*, *105*(A12), 27457–27468.

Parker, E. (1958). Cosmic-ray modulation by solar wind. *Physical Review*, *110*(6), 1445.

Reames, D. V. (2021). *Solar Energetic Particles. A Modern Primer on Understanding Sources, Acceleration and Propagation* (Vol. 978). doi: 10.1007/978-3-030-66402-2

Sabbah, I. (2000). The role of interplanetary magnetic field and solar wind in modulating both galactic cosmic rays and geomagnetic activity. *Geophysical research letters*, *27*(13), 1823–1826.

Shrivastava, P. K., & Jaiswal, K. (2003). High-speed solar wind streams and cosmic-ray intensity variations during 1991–1996. *Solar Physics*, *214*(1), 195–200.

Storini, M. (1990). Galactic cosmic-ray modulation and solar-terrestrial relationships. *Il Nuovo Cimento C*, *13*(1), 103–124.

Zyla, P., Barnett, R., Beringer, J., Dahl, O., Dwyer, D., Groom, D., ... others (2020). Review of particle physics. *Progress of Theoretical and Experimental Physics*, *2020*(8), 083C01.